International Journal of Naval Architecture and Ocean Engineering 14 (2022) 100487

Contents lists available at ScienceDirect

International Journal of Naval Architecture and Ocean Engineering

journal homepage: http://www.journals.elsevier.com/international-journal-of-naval-architecture-and-ocean-engineering/

System-level modeling of marine power plant with PEMFC system and battery

Kamyar Maleki Bagherabadi [a, *], Stian Skjong [b], Jogchum Bruinsma [c], Eilif Pedersen [a]

[a] Department of Marine Technology, Norwegian University of Science and Technology, Trondheim, Norway
[b] SINTEF Ocean, Ålesund, Norway
[c] Nedstack Fuel Cell Technology, Arnhem, the Netherlands

ARTICLE INFO

Article history:
Received 30 December 2021
Received in revised form
9 August 2022
Accepted 18 September 2022
Available online 29 September 2022

Keywords:
Marine hybrid power system
PEM fuel Cell system
System-level modeling
Averaged-value converter modeling

ABSTRACT

This article presents a model of a marine power plant with hybrid power sources consisting of Proton Exchange Membrane Fuel Cells (PEMFCs) and batteries. The primary objective is to develop a system-level fidelity model of the fuel cell-fed marine power systems with real-time capabilities. The model encompasses various mechanical and electrical domains such as the air-supply and the hydrogen auxiliary sub-systems of the PEMFC system, the power management system, the DC electrical converters with average - value assumptions and thruster and propeller dynamics. Moreover, the PEMFC system model in this work is verified and tuned with the experimental dynamic behavior of a PEMFC with a power capacity of 500 kW for specific applications in the marine sector. The presented model can be implemented for investigating the system performance for simulator applications, designing high-level controls, sizing and optimization. Indeed, the modular approach of the bond graph modeling strategy provides flexibility in the configuration and capacity of the power sources, as well as storage for further studies. Furthermore, this model of the fuel cell-fed power system is practical for feasibility studies of various maneuvering operations with a potential of integrating with the co-simulation applications. In the end, a simulation with torque set-points to the thrusters consisting of load steps and noises are proposed to evaluate the system performance, the controller robustness, and the high-level control performance in load sharing.

1. Introduction

Due to environmental issues, the International Maritime Organization (IMO) regulation directed the shipping industry and related research areas on all-electric vessels as a solution to reduce emissions (Lim et al., 2019). The electrical propulsion as a solution to these regulations becomes an effective configuration in the case of demanding significant electrical power on board. The demanded electrical power can be supplied by the hybrid power systems with mechanical or electrochemical sources as an efficient configuration with the energy storage components (Geertsma et al., 2017). The mechanical power is produced by the internal combustion engines and gas turbines converting the mechanical power to electrical power by the generators. The electrochemical power sources are fuel cells, which directly convert the electrochemical potential of the fuel to power electricity. The marine power plants are designed with various configurations and sizes according to the requirements. This endeavor demands feasibility studies and analyses for each alternative to achieve the best solution. For instance, the power can be supplied by the genset and fuel cells individually or in a hybrid configuration. The fuel cells are employed as either back-up, the auxiliary source or the main power supply in the vessels, which demands comprehensive understanding of the system's characteristics to decide on the proper configurations. The PEMFC system has gained more attention to be the primary power source of the vessels because of the high efficiency and zero-emission operation, which is aligned with current environmental issues and regulations (Van Biert et al., 2016). Fuel cells' potential is needed to be explored as the primary power source of the vessels through the aid of simulations and modeling.

Modeling and simulation as a practical tool provide a comprehensive understanding of the system's behavior in various

* Corresponding author.
E-mail addresses: kamyar.maleki@ntnu.no (K.M. Bagherabadi), stian.skjong@sintef.no (S. Skjong), Jogchum.Bruinsma@nedstack.com (J. Bruinsma), Eilif.Pedersen@ntnu.no (E. Pedersen).

Peer review under responsibility of The Society of Naval Architects of Korea.

https://doi.org/10.1016/j.ijnaoe.2022.100487

operations, which leads to a feasible and optimum design decision. However, the models have a wide range of fidelity, which defines the outputs' details and computational efforts. A compromise between the expected system model dynamics and computational time reaches a practical and efficient modeling approach to the problem. The marine power plant As a multi-domain system requires system-level modeling for analyses and feasibility investigations. The system-level fidelity models capture the necessary dynamics and facilitate the integration of components with less computational time compared with detailed models.

There are system-level modeling studies in the field of marine power plants, which are practical for analyses and design with an emphasis on the engine and generator sets as the primary power sources. In (Pedersen and Pedersen, 2012a), a flexible model library is developed for the all-electric vessel power plants with the bond graph method as the modular approach for modeling the multi-domain systems. The library contains engines, a fuel cell, a generator, electrical converters and motors, a ship model and propellers. The flexibility and modularity enable the library to be used for analyzing current cases while designing new power plants with various sizes and configurations. In (Ghimire et al., 2020), a dynamic model of the marine DC hybrid power system is proposed, which is verified by laboratory experimental results. The presented model is re-configurable due to the modular component modeling approach, with emphasizing on the electrical component physics.

The system-level modeling approach is presented in (Zahedi and Norum, 2012) for the marine DC hybrid power system by considering the electrical and mechanical components. The vessel hydrodynamics and propulsion system with the reduced order assumptions are considered in the simulation. The main power sources in this work are diesel engines and generators. Furthermore, in (Shajari et al., 2020) a system-level model of a power plant consists of a diesel generator, a battery and a Solid Oxide Fuel Cell (SOFC) with the average - value assumption for the electrical and mechanical components. The model is developed practically for the system's dynamic performance investigations in the various operational conditions. Also, in (Zhu et al., 2018) a ship-wide system-level model is proposed that contains the electrical and mechanical physics to investigate the system's behavior in an effective manner from a computational time point of view. The numerical stability and control issues of the generator models with a generic modeling framework for a weak grid marine power plant are studied and illustrated in (Skjong and Pedersen, 2017). The model has the real-time capabilities of the power system model, which is integrated into the vessel dynamics models for co-simulation studies (Skjong et al., 2018).

There are limited studies on the dynamic modeling of fuel cells as the main power source of the marine power plant. A multi-domain dynamic model of a Molten Carbonate Fuel Cell (MCFC) system is developed and verified by (Ovrum and Dimopoulos, 2012) to help facilitate the design and approval of employing the MCFC for the auxiliary power source of an offshore supply vessel. PEMFC in the marine sector has gained more attention for further zero emissions studies among the fuel cells. A model of PEMFC and a super capacitor is proposed for small ships in (Benyahia et al., 2012). The primary aim of the work is to investigate super capacitor performance in hybrid power systems to improve the slow dynamics of PEMFC. Indeed, a model of a marine hybrid power system by (Chen et al., 2020) is presented with the PEMFC and genset with an equivalent equal circuit model assuming average - value assumptions for the power converters.

The PEMFC has attained more attention in research studies to be utilized as the primary power source in the vessel power plant. This endeavor can be facilitated with a validated high fidelity PEMFC system model of the marine application in integration with other power system components. Indeed, the generic view and flexibility in size and configuration enable the feasibility studies in the design stage. Regarding the above literature, there are some studies on integration equivalent circuit model of PEMFC with small scale laboratory validation with other electrical components and battery in hybrid power system. However, there is a gap in providing a generic hybrid power system model with emphasis on high fidelity validated PEMFC system model for marine application as the primary power source in integration with a battery as the energy storage and other electrical components.

This work proposes a system-level fidelity model of the hybrid power system with a validated high fidelity PEMFC system for marine application and a battery. The electrical and mechanical components of the system are considered with physical relations. Indeed, power electronics converters are estimated by the average - value relations. The average - value assumption for the electrical converters decreases computational time significantly. However, the accuracy of the results is in good agreement with waveform level models (Zhu et al., 2018). This work aims to develop a model that fills the gap in the generic modeling of hybrid power plants with verified PEMFCs for marine applications and batteries with a modular approach and real-time capabilities. The developed PEMFC system consists of auxiliary components, and the static and dynamic behaviors are validated against a PEMFC system vendor for marine applications. Therefore, this model estimates PEMFC's performance as the primary power source component due to employing experimental data of the FC, which can be installed on board. The modular modeling approach provides flexibility in the power system configuration and the power management system can be tuned for various number of components and sizes. The vessels have a wide range of power sizes and configurations. This model can be used for feasibility studies in designing or retrofitting. The model's real-time capabilities facilitate system integration into the thrusters' model, the vessel dynamics model and energy and power management systems with co-simulation approach. Bond graph as a multi-domains and modular modeling strategy is employed for this work (Karnopp et al., 2012).

1.1. Article outline

In Section 2, the modeling approach and equations with the bond graph implementation for the system's mechanical and electrical components are presented. In Section 2.1, the model of the PEMFC system is developed with an emphasis on the air supply sub-system, which has the most effect on dynamics, and the system efficiency. The PEMFC system validation and tuning by the experimental data with the polarization and transient curves are represented in Section 2.3. The battery, converters and controller model developments and relations are described in Section 2. The simulation scenario and results are illustrated and discussed in Section 3.2. In the end, the conclusion is presented in Section 4.

2. Modeling

Fig. 1 illustrates the single line diagram of the modeled power plant with full-converter-based DC integration configuration (Haxhiu et al., 2020). The system consists of the PEMFC system, the battery, converters, inverters, electrical motors and propellers, and includes various physical domains. This work is developed based on two main assumptions in the modeling approach. First, the mechanical components are modeled with system-level fidelity and physical assumptions. For example, the PEMFC system has lumped control volumes for the stack and air supply sub-systems. Second, the performance of the electrical components is modeled with the average - values assumption for the high frequency switching

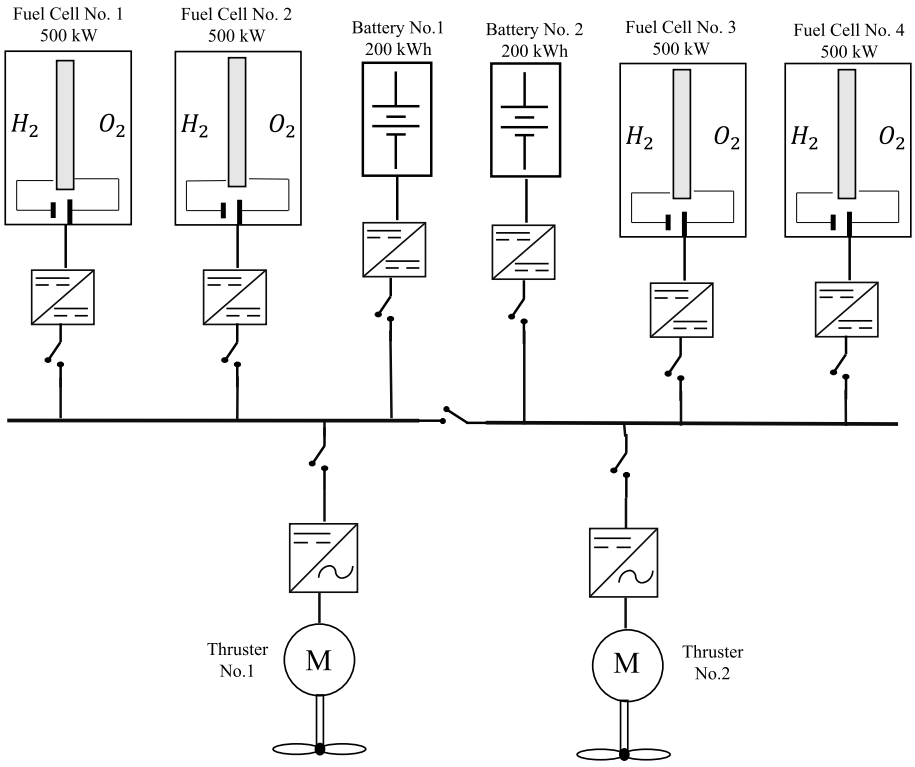

Fig. 1. Single line diagram of the modeled vessel power plant with hybrid power sources consist of the PEMFC system and the battery.

behavior. Thus, the computational efforts are reduced, while the required details are maintained. As mentioned earlier, the ship power plant consists of various physical domains with power conversions. Consequently, the bond graph (Karnopp et al., 2012) approach, as a multi-domain energy based modeling strategy, is utilized for this work. The modular view of the bond graph facilities the model flexibility for various configurations.

The system is divided into components with detailed mathematical relations, which are presented individually in the following subsections. The PEMFC is the system's primary power source, and the batteries are the energy storage.

2.1. PEMFC system

The PEMFC system shown in Fig. 2 consists of the stack, the air supply sub-system, the hydrogen supply sub-system and the thermal management sub-system. The stack, the heart of the fuel cell, converts the chemical energy of the supplied hydrogen and oxygen to the electrical power directly. The electrical efficiency and dynamics of the system are dependent on supplying the two reactants. Therefore, the auxiliary sub-systems play an important role in the system operating characteristics. In this model, the net system efficiency and dynamic responses in the order of seconds are the primary focus of the PEMFC model. Among the auxiliary systems, the air supply system, which consists of the blower, manifolds and cathode affects the net system efficiency and dynamic responses the most. The dynamic response of the air supply subsystem is in the order of seconds (Pukrushpan et al., 2004), which is important to be considered in the system-level modeling approaches. The hydrogen is supplied by a high pressure tank and a

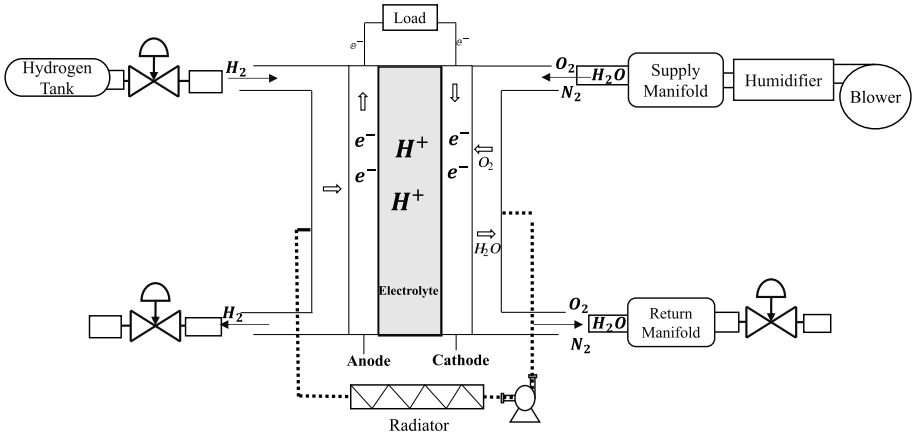

Fig. 2. Schematic of the PEMFC system with auxiliary sub-systems and chemical reactions in the stack.

control valve, which simultaneously adjusts the required pressure. Hence, the dynamic of the hydrogen supply section is small enough to be neglected. The thermal management sub-system responds to the temperature variations in the order of minutes, which can be neglected in system-level considerations (Vasu and Tangirala, 2008). Thus, in this model, besides the stack with the anode and cathode, the physics of the air supply, the cathode, the hydrogen supply and the anode for a more realistic estimation of the efficiency and dynamics are considered.

2.1.1. Stack and cell model

The cell voltage v_{cell} is obtained from Eq. (1). The overpotentials are activation voltage v_{act}, ohmic voltage v_{omh} and concentration voltage v_{omh}, which are subtracted from Nernst voltage v_{Nernst} as the reversible potential. The overpotentials are estimated by curve fittings to the experimental data. These values are dependent on the operational parameters such as the partial oxygen pressure, the stack temperature and the load. The detailed relation of the Nernst and chemical potential are given in the Appendix.

$$v_{cell} = v_{Nernst} - v_{act} - v_{omh} - v_{con} \tag{1}$$

The activation voltage is considerable on the low load and by increasing the load, it becomes constant. The characteristic of this over voltage is estimated by Eq. (2a). Where T_{st} is the stack temperature, $T_{ref} = 298$ K is the reference temperatures, p_{ca} is the cathode pressure, p_{O_2} is the partial pressure of oxygen and p_{sat} is the water saturation pressure (Pukrushpan et al., 2004). a_{ij} as constant coefficients must be tuned according to the experimental data of the polarization curve.

$$v_{act} = v_0 + v_a(1 - e^{-c_1 i}) \tag{2a}$$

$$v_0 = a_{11} + a_{12}\left(T_{st} - T_{ref}\right) + a_{13}T_{st}\times \left[ln\left(\frac{p_{ca} - p_{sat}}{a_{14}}\right) + \frac{1}{2}ln\left(a_{15}\frac{p_{ca} - p_{sat}}{a_{14}}\right)\right] \tag{2b}$$

$$v_a = (a_{21}T_{st} + a_{22})\left(\frac{p_{O_2}}{0.1173} + p_{sat}\right)^2 + (a_{23}T_{st} - a_{24})\left(\frac{p_{O_2}}{0.1173} + p_{sat}\right) + (a_{25}T_{st} + a_{26}) \tag{2c}$$

The charge transfer through the membrane causes resistance, which is ohmic over voltage representing this electrical loss. The ohmic over voltage is obtained from Equation (Pukrushpan et al., 2004). where t_m is the membrane thickness and λ is a non-dimensional parameter to demonstrate the relative humidity of the membrane, which is considered $\lambda = 14$ to induce 100% relative humidity of the membrane. The ohmic voltage has linear behavior and is dominant on the middle load range. The constant parameters b_{ij} are tuned regarding the proper fitting of the polarization curve.

$$v_{ohm} = i \cdot R_{ohm} \tag{3a}$$

$$R_{ohm} = \frac{t_m}{\sigma_M} \tag{3b}$$

$$\sigma_M = (b_{11}\lambda + b_{12})exp\left(b_{13}\left(\frac{1}{b_{14}} - \frac{1}{T_{st}}\right)\right) \tag{3c}$$

The concentration voltage is considerable in current densities. Eq. (4) obtains the concentration over voltage as function of current.

$$v_{conc} = i\left(c_2\frac{i}{i_{max}}\right)^{c_3} \tag{4}$$

The cells could be connected in series and parallel configurations to produce the demanded voltage and current range in the stack. In this system, the cells have similar performance and voltage responses. The fuel cell voltage v_{fc} obtained from Eq. (5) and $N_{cell_{Series}}$ is the number of cells in series. The fuel cell load range I_{fc} is calculated from Eq. (6) and is the number of cells in parallel.

$$v_{fc} = N_{cell_{Series}} \times v_{cell} \tag{5}$$

$$I_{fc} = N_{cell_{parallel}} \times I_{cell} \tag{6}$$

The fuel cell net power p_{fc} is achieved from Eq. (7). The reactants are supplied by auxiliary components that consume a considerable amount of power. The power consumed by the auxiliary components p_{aux} is considered to obtain the fuel cell net power. The estimated consumed auxiliary power varies with the load range.

$$p_{fc} = v_{fc} \times I_{fc} - p_{aux} \tag{7}$$

2.1.2. Air supply sub-system

The air supply system consists of the blower, manifolds and the cathode. The blower inertia and air filling of the volumes cause time responses in the order of seconds. The manifolds are modeled with C-elements as shown in Fig. 3. In this model, the ideal gas relations are assumed for the air supply and control volumes for the thermodynamics calculations. The partial pressures of oxygen, nitrogen, water vapor and air pressure are calculated by Eq. (8). In Eq. (8) R_a is the air gas constant, T is the control volume temperature, V is the volume of the manifold or the cathode and $\dot{m}_{in,out}$ represents the inlet and outlet mass flow rates to the control volumes. The cathode pressure p_{ca} in Eq. (9) is the summation of the partial pressure of oxygen p_{O_2}, nitrogen p_{N_2} and water vapor p_{H_2O}.

$$\frac{dp}{dt} = \frac{R_a T}{V}\left(\dot{m}_{in} - \dot{m}_{out}\right) \tag{8}$$

$$p_{ca} = p_{O_2} + p_{N_2} + p_{H_2O} \tag{9}$$

The valves' mass flow rates are predicted with both linear and nonlinear relations. In the case of small pressure differences between the reservoirs, such as the cathode inlet valve, the linear correlations are valid. In Eq. (10), $\dot{m}_{c,in}$ is the estimation of the mass flow rate, k_{cons} is a constant coefficient and p_{sm} is the supply manifold pressure (Pukrushpan et al., 2004). However, in the case of considerable pressure differences, similarly to the return manifold valve, the nonlinear rations are employed and can be found in the Appendix.

$$\dot{m}_{c,in} = k_{cons}(p_{sm} - p_{ca}) \tag{10}$$

Fig. 3 depicts the causality of the system from signal to the electrical motor until load. The torque of the electrical motor, the rotational speed of the electrical motor and the torque of the blower are obtained from Eq. (11).

$$\tau_{em} = \eta_{em}\frac{k_t}{R_{em}}(v_{em} - k_v\omega_{bl}) \tag{11a}$$

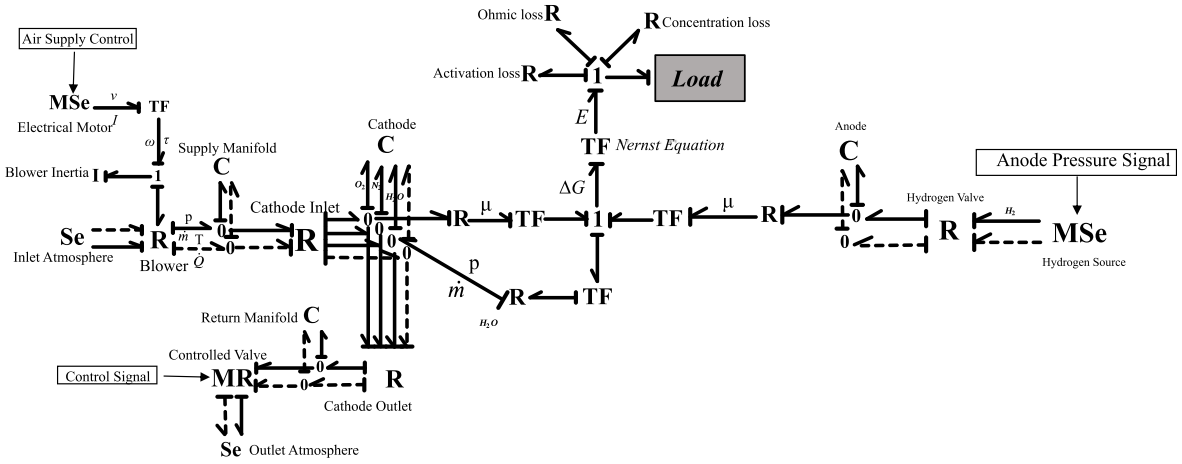

Fig. 3. Bond graph model of PEMFC system with constant temperature assumption.

$$J_{bl}\frac{d\omega_{bl}}{dt} = \tau_{em} - \tau_{bl} \tag{11b}$$

$$\tau_{bl} = \frac{C_p}{\omega_{bl}}\frac{T_{ref}}{\eta_{bl}}\left[\left(\frac{p_{sm}}{p_{atm}}\right)^{\frac{\gamma-1}{\gamma}} - 1\right]\dot{m}_{bl} \tag{11c}$$

where τ_{em} is torque of the electrical motor, v_{em} is the input voltage to the electrical motor, J_{bl} is the rotational inertial of the blower, $\dot{m}_{bl}$ is the air mass flow as the output of the blower, $\dot{m}_{bl}$ is the mass flow rate of the blower and p_{sm} is the pressure of the supply manifold. The constant parameters are scaled by the method described in details in (Bagherabadi et al., 2022). The parameters are given in the Appendix based on (Pukrushpan et al., 2004) (Bagherabadi et al., 2022).

2.1.3. Hydrogen supply sub-system

The dynamics of regulating the desired pressure in the anode are fast enough to be neglected in the system-level modeling based on (Pukrushpan et al., 2004). In this model, the hydrogen supply as shown in Fig. 3 is modeled with an ideal hydrogen source, a valve and the anode reservoir. The same relations of the valve and the reservoir in the cathode are employed for the anode. The demanded hydrogen pressure is adjusted regarding the air pressure in the cathode.

2.2. Control of the PEMFC system

The control schematic of the PEMFC is shown in Fig. 4. λ_{O_2} is the oxygen excess ratio, which is defined as the ratio of oxygen consumption to that supplied. Increasing the load decreases the oxygen excess ratio, which can cause starvation. By regulating the blower voltage, the PI controller adjusts the excess ratio to the commanded set point.

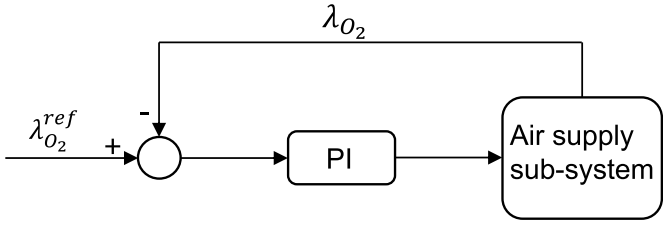

Fig. 4. The control schematic of the air supply system.

2.3. Validation and tuning of the PEMFC system

The PEMFC system in this work is calibrated with Nedstack PEMFC stacks and modules in both the static and dynamic operations. These PEMFC systems are designed and manufactured for maritime applications (Smit, 2014). The operational parameters and the system specifications of the PEMFC system for the validation are given in Table 1. The polarization curve validation is shown in Fig. 5. The static behavior of the stack is validated by tuning the parameters of the electrical losses. As mentioned, the beginning of the polarization curve is affected by activation loss, so adjusting the activation loss coefficients results in the curves' agreement with the low load. Afterward, to validate the mean load, the parameters of the ohmic loss area adjusted. There is a good agreement between the reference and the tuned model in the static behavior.

The dynamic response of the system is also calibrated with reference experimental data as is shown in Fig. 6. The primary parameters for dynamic validation are the supply manifold and stack volume, the blower inertia, and the coefficient of the cathode outlet vale. These parameters are tuned to obtain a close voltage response to the reference, and cathode and manifold pressures do not exceed 1.2 bar. There is acceptable agreement with the model time responses and experimental data.

2.4. Lithium ion battery model

The equivalent circuit of a high power lithium ion battery is modeled and developed according to the provided experimental

Table 1
The operational parameters and system specification of the PEM fuel cell system for validation.

Parameter	Description	Value
T_{st}	Temperature of the stack	65
λ_{O_2}	Stoichiometry of air	2.0
λ_{H_2}	Stoichiometry of hydrogen	1.25
λ	Non-dimensional parameter of the membrane relative humidity	14[100%]
V_{st}	The operational voltage range	500 − 1000 [V]
I_{st}	The operational current range	0 − 1200[A]
N_{cells}	Number of cells	60 × 96

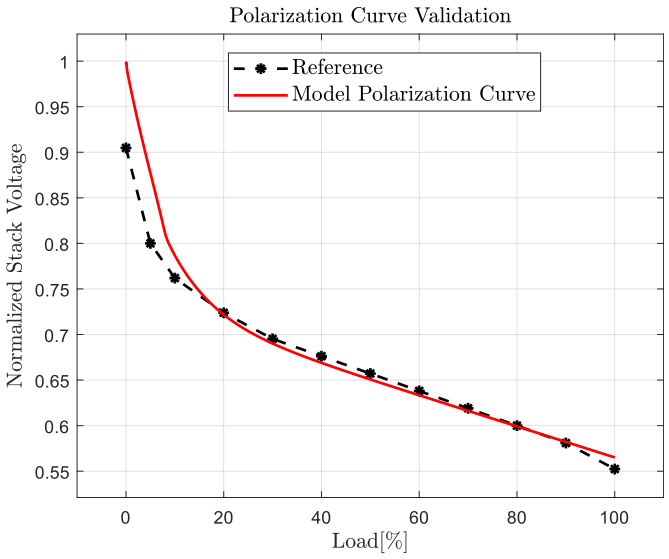

Fig. 5. The polarization curve validation.

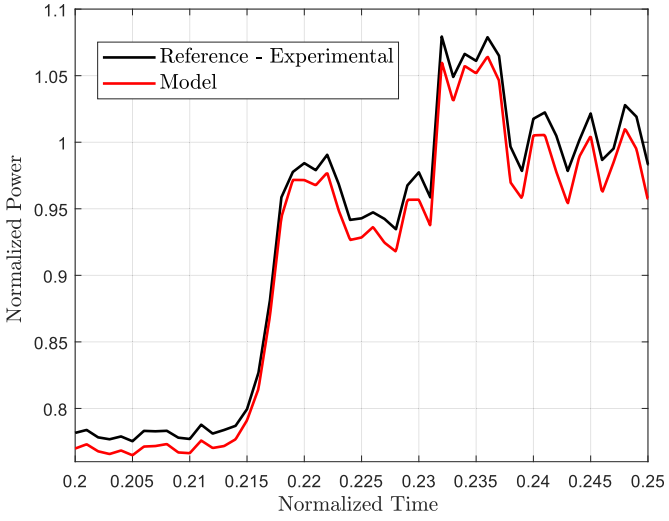

Fig. 6. The dynamic response validation.

data in (Huria et al., 2012). The electrical circuit is shown in Fig. 7 which is implemented as a bond graph model. The open circuit voltage is dependent on the resistance and R_0, R_1, C_1 and E_0, which are functions of the temperature and the state of charge (SOC). The parameters' dependencies are estimated with a fifth-order polynomial curve fitting to the provided experimental data in (Huria et al., 2012). The battery cells are configured in series and in parallel to produce the demanded voltage and the current range from the battery pack. The total battery power $p_{battery}$ is calculated from the battery voltage $V_{battery}$, the battery current $I_{battery}$ and the number of cells N_{cells} in Eq. (12).

$$p_{battery} = V_{battery} \times I_{battery} \times N_{cells} \tag{12}$$

The battery cell temperature T_{cell} is calculated from Eq. (13), which is an energy balance between natural convection and the produced heat of the internal battery cell resistance. $hA = 0.51 \mathrm{WK}^{-1}$ is the heat convection and the surface area of the heat transfer, $C_T = 2.04 \times 10^6 jm^{-3}K^{-1}$ is the heat capacity of the cell and $T_{air} = 298$ K is the air temperature (Huria et al., 2012). The produced heat by the battery because of resistances is obtained from Eq. (14). Where V_0 is the voltage of resistance R_0 and V_1 is the voltage of resistance R_1.

$$\frac{dT_{cell}}{dt} = \frac{hA}{C_T}(T_{air} - T_{cell}) + \frac{1}{C_T}Q_{El,resistance} \tag{13}$$

$$Q_{EL,resistance} = V_0 I + V_1 I \tag{14}$$

The battery state of charge is calculated from Eq. (15). When the SOC is 0, it shows that the battery is empty, while SOC 1 shows the battery is fully charged. $Q_{battery} = 31$ Ah is the cell battery charge capacity, with the integration of the battery current depicting the consumed or stored charge in the cell Eq. (15a).

$$Q_e(t) = \int_0^t I_{battery}(\tau)d\tau \tag{15a}$$

$$SOC = 1 - \frac{Q_e}{Q_{battery}} \tag{15b}$$

(a) Electrical circuit diagram of the modeled battery (Huria et al., 2012) (b) The bond graph implementation of the modeled battery].

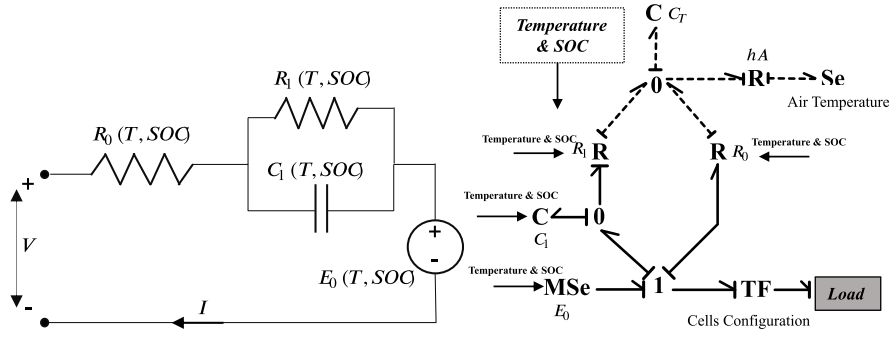

(a) Electrical circuit diagram of the modeled battery [20] (b) The bond graph implementation of the modeled battery

Fig. 7. The modeled battery with effect of temperature.

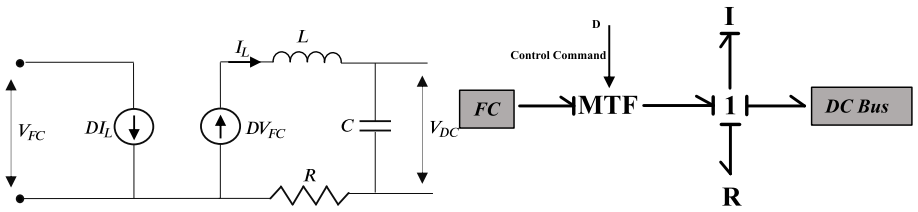

(a) Electrical circuit diagram of the modeled buck converter (b) The bond graph representation of the modeled buck converter

Fig. 8. The buck converter electrical circuit and bond graph representation.

2.5. Power electronics converters

The fuel cells, batteries and propulsion motors are connected to the DC bus through power electronic converters. The converters are employed for the power control of the fuel cells, as well as the bus voltage regulation. The converters operate based on high frequency switchers; however, the average - value relations are assumed in this work. This simplification does not affect the dynamics from the system-level modeling, as the average - value relations are assumed, despite the reduction of the computational effort significantly.

2.5.1. DC-DC buck converter

The fuel cell power is controlled by a DC-DC converter. In this work, an average model of the buck converter is developed, as shown in Fig. 8. The average model substitutes the switches and rectifier operation by the duty ratio (D). This assumption reduces the computational effort and increases the model solver's robustness. The dynamics of the switches are fast enough to be neglected in the ship-wide system-level modeling (Janke, 2015) (Chen et al., 2020).

As shown in Fig. 9, the closed loop PI controller is considered for controlling the fuel cell power. The controller regulates the duty ratio to achieve the power set point defined by the power management system.

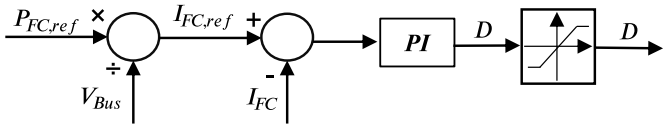

Fig. 9. The buck converter control strategy.

2.5.2. DC-DC converter bi-directional

As energy storage, the battery requires two side power flows for charging and discharging. In this work, a bidirectional DC-DC converter with buck-boost modes and an average - value assumption is proposed. The equivalent circuit and bond graph representation are shown in Fig. 10. The switch and diode operations are modeled with average - value assumptions. Regarding the duty ratio from controller, the modular transfer components *MTF* as a bond graph element induces the voltage difference to the inductor. The voltage difference produces the current for the charging or discharging according to the sign of voltage difference (Arabul et al., 2015).

The control strategy for the bidirectional converter is shown in Fig. 11. The control strategy for this converter is PI voltage based (Zhang et al., 2020).

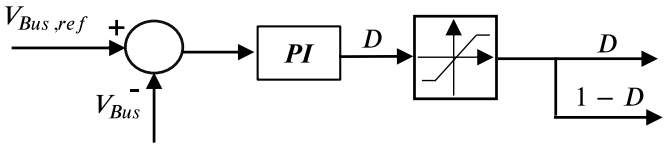

Fig. 11. The bidirectional control strategy.

2.5.3. Power management control strategy

Fig. 12 shows the power management control strategy for the fuel cells. The load demand is passed from the low pass filter, while the low frequency loads are compensated with fuel cell No.1. The other fuel cells just start sequentially on their operating set point for the higher load demands. Indeed, the high load frequencies and oscillations are supplied by the batteries to maintain the bus voltage constant. In case of decreasing the mean load, the fuel cells will be shut down sequentially. The low pass filter causes a delay to compensate the demanded load by fuel cells. Thus, the battery controller is based on the bus voltage and provides the load demand until the fuel cell approach the defined power set point. The demanded load passes through low-pass filter to be decomposed to the high and low frequency. The cut-off frequency defines the imposed load on the battery and the fuel cell. A compromise between battery storage capacity and smooth load on the fuel cell has to be considered to design a proper filter (Nehrir and Wang, 2009). In this case, one step load is passed from the filter, and the cut-off frequency is adjusted in a way that the imposed load to the battery maintains the charge and discharge rate limitations.

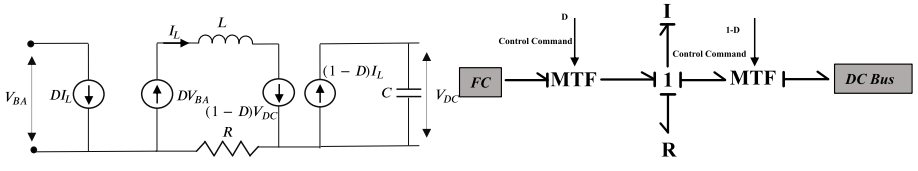

(a) Electrical circuit diagram of the modeled battery [20] (b) The bond graph implementation of the modeled battery

Fig. 10. The modeled bidirectional DC-DC converter.

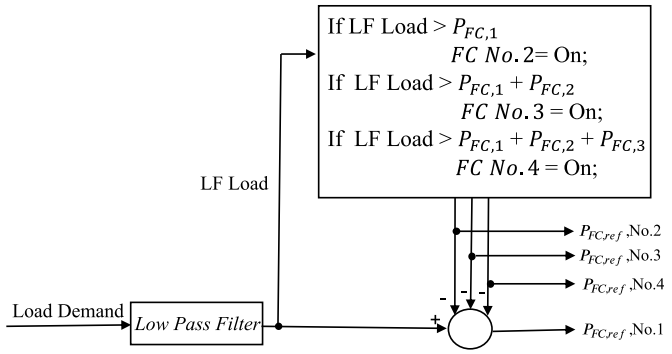

Fig. 12. The power management control strategy of the fuel cells.

2.5.4. Voltage source inverter model

The average model assumption for the voltage source inverter based on (Zahedi and Norum, 2012) is implemented in Eq. (2.5.4), where V_{DC} is the DC bus voltage, I_{DC} is the imposed current to the power system, m is the modulation index, φ_2 is the initial phase angle and φ is the d-q transformation angle. The parameters in Eq. (2.5.4) are defined by the controller in the thruster model in Section 2.6.

$$\begin{bmatrix} v_q \\ v_d \end{bmatrix} = \begin{bmatrix} sin(\varphi_2 - \varphi) \\ cos(\varphi_2 - \varphi) \end{bmatrix} mV_{DC} \tag{16a}$$

$$I_{DC} = m\left((i_q sin(\varphi_2 - \varphi)) + i_d cos(\varphi_2 - \varphi)\right) \tag{16b}$$

2.6. Thrusters

The thruster contains a propeller, an induction motor and a frequency converter to control the propeller torque. The implemented model in this work is from the NTNU marine vessel bond graph model library developed by Pedersen et al. (Pedersen and Pedersen, 2012b). The thrust is calculated by Eq. (17) and the torque is obtained from Eq. (18) (Sørensen, 2005).

$$T_a = sign(n) k_T \rho_w D^4 n^2 \tag{17}$$

$$Q_a = sign(n) k_Q \rho_w D^5 n^2 \tag{18}$$

where n is the rotational speed, ρ_w is density of water, D is the diameter of the propeller, K_T and K_Q are the thrust and torque coefficients respectively. The induction motor of the thruster is connected to the DC bus by the inverter. The torque set points of the thruster and water velocity are the inputs of the thruster and the required electrical power of the induction motor as output, which is supplied by the power system.

2.7. Validation

The validation of a model is defined as the accuracy level of estimations of the model regarding primary intentions and expectations by the simulation (Vrijdag et al., 2009) (Schuddebeurs et al., 2008). Marine ship-wide models consist of various physics and domains that the validation of the whole system is a challenge due to complexity or lack of data for being in design stage (Schuddebeurs et al., 2010; Bø et al., 2015). However, the submodels and the integration can be validated individually by considering the dynamic and static behaviors (Schuddebeurs et al., 2010) (Zahedi, 2014). The transient time of the marine power plant subsystems is shown in Table 2. In a system-level and simulators the dynamics at the order of milliseconds and seconds are demanded to be captured by the model. The power system consists of fuel cells, batteries, converters and switchers. Switchers and other electrical components have time transients on the order of microseconds. The average value assumption is a reasonable estimation for this work. Therefore, the dynamics of the fuel cell and battery affect the whole system on the order of milliseconds and second, which is the primary focus in system modeling. In this work, the fuel cell dynamics and static responses are validated against experimental data, as the main aim of developing a hybrid system based on PEMFCs for design and feasibility studies. The battery and other electrical components are modeled based on physical relations and experiments with references. Indeed, the integration of the components and submodels is based on the bond graph approach based on energy conservation. According to the components validations and energy-based integration, it is concluded that the model may estimate the system behavior with a good agreement.

Table 2
The time scale of marine power plants submodels (Schuddebeurs et al., 2010; Bø et al., 2015).

subsystem	Time scale
Power converters switching	1 – 5 μs
Thruster drive	10 ms–1 s
Battery charging	10 ms–1 min
PEMFC system unit	500 ms–1 min
Propeller inertia	1 s–10 s

3. System simulation

In Section 2, the modeling approach and relations of the electrical and mechanical components according to the system characteristics are presented. Indeed, the PEMFC system is tuned and verified against the experimental data. The implemented PEMFC is designed and manufactured for marine applications, which provides a more realistic estimation of the fuel cell behavior in various vessel operations and load demands. The simulation is designed to investigate the fuel cells, the batteries and controllers' performances in the various load levels with fluctuations. The simulation scenario and results are discussed in the following. The schematic of the model causality and the interaction of the components during simulation is depicted in Fig. 13. The torque set-points and water velocity are the inputs to the model. The corresponding current to torque and velocity is induced on the DC link. The PMS decides on the load share regarding the algorithm in Fig. 12 by defining the power set points to the battery and fuel cells. The fuel cells operational conditions are the same as the validation condition in Table 1. The simulations were performed by 20-sim as a solver for the bond graph models. 20-sim as a modeling and simulation software supports bond graph, block diagrams, equations, and Functional Mock-ups (FMU). The solver has sophisticated numerical integration methods for stiff problems, which is advantageous for modeling the dynamic behavior of the engineering systems (Broenink, 1999).

3.1. Simulation scenario

In this scenario, five load step-ups are implemented as the torque reference set points to the thrusters with noises as the wave loads. Besides, two step down loads are applied for checking the

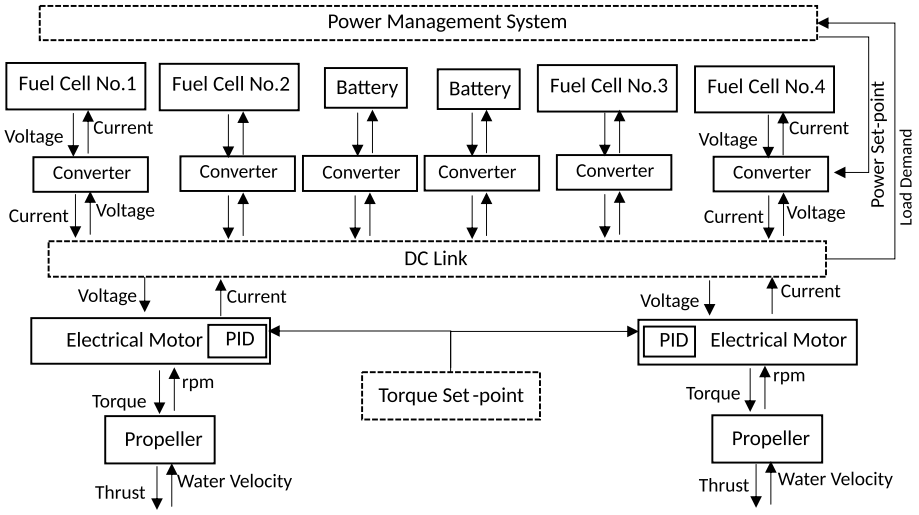

Fig. 13. The simulation flow chart and the causality of the components.

turning off of the fuel cells' effects on the bus voltage. Also, the step loads are designed to test the robustness of the control system to maintain the bus voltage through the defined set points. The noises are considered to check the low pass filter and battery behavior for supplying the load fluctuations. The noise has the maximal frequency of 4 Hz to simulate the worst situations that the system may encounter in future works. The load demands initiate with idle to allow the system to stabilize. The step loads are then applied with the time domain of $t = 100\ s$. The peak load occurs from $t = 400\ s$ until $t = 500\ s$, which is the maximum power demand. The system initiates with an idle load demand to allow the system primary numerical convergence. At $t = 50\ s$ the first load ramps applied. The load increment is supplied by the battery and fuel cell No.1 simultaneously. However, the fuel cell has slower dynamics regarding the battery, so having a high discharge rate compensates for the step initially. Afterward, the fuel cell follows the average load, while the battery discharge rate is decreased and just supports the fast dynamic power demands. Afterward, at $t = 100\ s$ another load step is demanded; hence, the battery supplies the initial ramp. However, the average load value is more than one fuel cell's power capacity. Thus, fuel cell No.3 starts at the determined load set-point. This fuel cell operates at a constant load, with the difference in the load demand and this fuel cell supported by fuel cell No.1 in the part load mode. At $t = 200\ s$, the loading ramp does not reach the load capacity of two fuel cells, so fuel cell No.1 compensates for the load by increasing the power. From $t = 400\ s$ until $t = 500\ s$ the load demand is approximately 1.3 MW, and four fuel cells and the battery operate to meet the load demand. Three of the fuel cells operate at the constant operational set-point. From $t = 500\ s$ two step downs are required in load demands; at this time, fuel cell No.4 shuts down and the battery converts to charging mode to help compensate the transient. Consequently, other constant load fuel cells are shut down. Afterward, two step downs are applied to the system to check that the fuel cells have shut down and the effects on the system's robustness. In summary, the simulation scenario consists of the increasing and decreasing of the load with steps and oscillations.

3.2. Simulation results

In this section, the results from the simulation are illustrated and described. The step loads and water velocity are the inputs to the model. These inputs are applied to the thruster, which the induction motor produces for the torque set points. The induction motor through the inverter induces the load demand to the power system. The model has two thrusters with the same performance and the same torque set point commands. The thrust and electromagnetic torque of the induction motor are shown in Fig. 14. The torque set points are followed by the electrical motor in a good agreement. The torque set points are the inputs to the system and produced thrust as the output regarding the water velocity. The water velocity fluctuates as the waves to the propellers cause fast variations in the thrust. These variations are designed to check controller stability in maintaining the bus voltage and the battery behavior to supply high frequency loads.

The power distribution of fuel cells, the battery and the load demands are shown in Fig. 15. According to the load levels, the fuel cells start sequentially in the determined operating set-points to supply the mean loads. However, one of the fuel cells is defined to operate in a part load to decrease the stresses on the battery. Therefore, fuel cell No.1 satisfies the low frequency loads, which decreases the high charge and discharge of the battery. Once, the load demand decreases the fuel cells shut down. In the ramps, the fuel cell start and shut down have a short time transient. These transients are supplied or absorbed by the battery as shown in Fig. 15. The first step up is at $t = 50$ s with load oscillations. The load steps are applied gradually to check the starting of the fuel cells. In the step load demands, the battery has a high discharge rate to supply the load to regulate the bus voltage to the defined set-point.

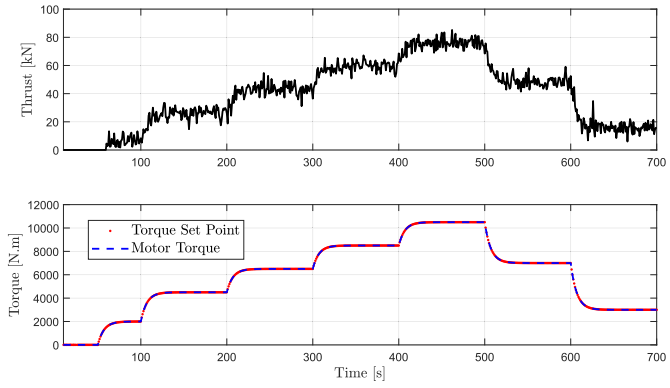

Fig. 14. The torque set points and the produced thrust.

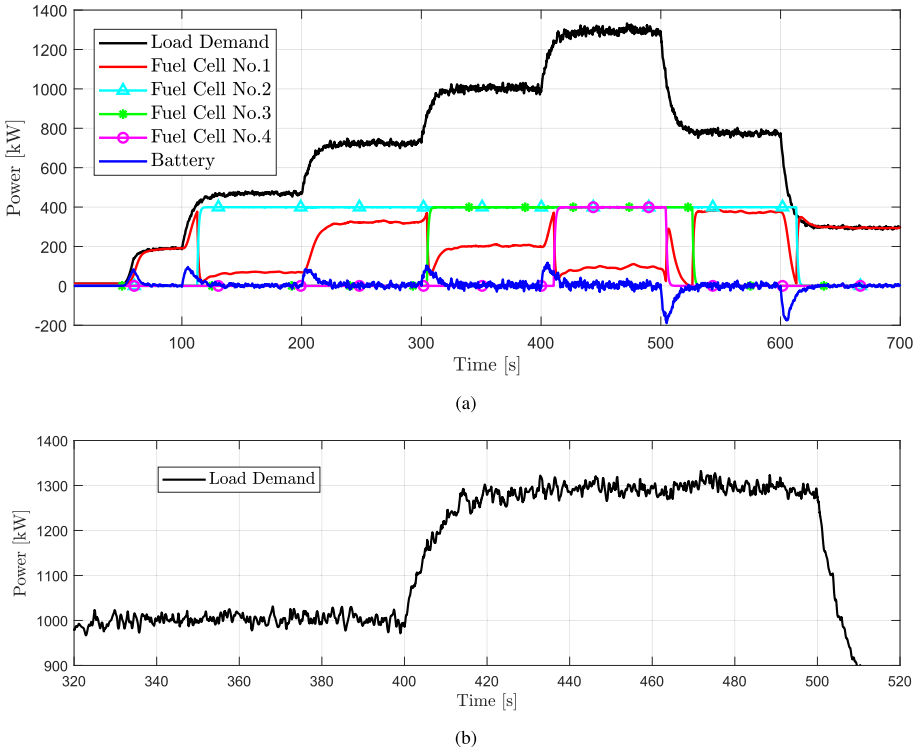

Fig. 15. (a) The load demand and load-sharing among the fuel cells and the battery, (b) Magnified load demand in the time domain.

Also, in the fuel cells shut down, the battery operates in charging mode to save the supplied energy and maintain the bus voltage. At high torque levels, the system requires excessive electrical power, so the fuel cells and battery supply the demanded load in parallel. It can then be concluded that the high-level control properly decides according to the load demand level. The battery also supports the high-frequency loads properly. Indeed, fuel cell No.1 supplies the part load (low frequency) as well.

At $t = 100$ s, the second step of the torque demands is applied and demands around 500 kW electrical power. This amount is more than 400 kW of ful cell No.1 power capacity, so fuel cell No.2 starts on 400 kW constant load. Then the load on fuel cell No.1 is reduced because it is aimed to supply the part load. From 200 s until 300 s fuel cell No.2 and No.1 produced the demanded load and the applied torque set point requires around 700 kW electrical power. So, it is under the capacity of two fuel cells. Afterward, the applied load at 300*s* increases the power demand up to 1000 kW. Therefore fuel cell No.3 starts on the constant load same as fuel cell No.2 and fuel cell No.1 supplies the part load. The starting of the fuel cells on constant load to compensate for mean load causes reduction with step down for fuel cell No.1. From $t = 400$ s until $t = 500$ s has the highest load demand, which is supplied by three fuel cells on the constant load and fuel cell No.1 on the part load. In later steps, the mean load is decreased and constant load fuel cells are turned off according to the PMS rule-based algorithm. The shut down of the fuel cells at 500 s and 600 s causes charging of the battery and sudden compensation by fuel cell No.1. Because the dynamic response of the fuel cells is lower than the batteries, the battery charges the extra power to maintain the DC bus voltage around the defined set point.

The bus voltage is shown in the upper plot in Fig. 16. The mean load is supplied by the fuel cells, and the oscillations are taken care of by the batteries with the bus voltage set point for the battery's converter. The control system of the bidirectional battery converter maintains the bus voltage within the desired set point. However, there are some dips less than 1% due to oscillations in the high level load, which are within the acceptable tolerance. Consequently, it shows the stability of the power system and DC bus voltage controller.

The battery power is shown in the second plot in Fig. 16. The battery supplies the fast transient load changes. Indeed, the sign of power is positive in discharging, the positive power flow direction is assumed to the bus. Hence, the negative power is the battery charging. The charging and discharging reach a C-rate of less than 1 in this simulation, which is applicable for the battery. Employing the fuel cells for the mean value load and one fuel cell for the low-

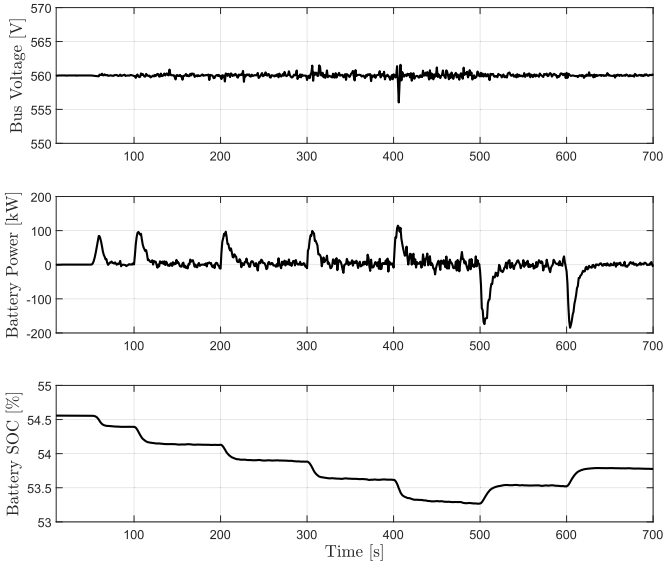

Fig. 16. The bus voltage, battery power and battery state of charge.

frequency loads decreases the high charge and discharge power flow of the batteries. The battery's highest charge and discharge rate are caused by the starts and stops of the fuel cells. In addition, the steps up of the load are faster than the dynamics of the fuel cell, and the battery supplies the sharp load increment to allow the fuel cell reaches the demanded load level. For example, at $t = 200$ s, the load step is applied, and the battery by simultaneous discharge, produced the demanded load until the fuel cell No.1 reaches the required load. Afterward, the battery load is maintained around zero and supplies the fast oscillations. At $t = 500$ s and $t = 600$ s two negative power demands as charging are caused due to the shut down of the fuel cells.

The battery state of charge is shown in the last plot in Fig. 16, with the effects of step loads in charging and discharging. The oscillations have high frequencies and low magnitudes. As a result have minor effects on the SOC.

The voltage of fuel cell No.1 is shown in Fig. 17, which supplies the low-frequency loads. The fuel cell properly follows the implemented load. At $t = 500$ s, the mean load is starting to decrease from 1300 kW to 800 kW, so fuel cell No.4 is shut down. Hence, fuel cell No.1 supports the part load until the load again decreases, and fuel cell No.2 is also shut down. So, the part load of fuel cell No.1 again is increased.

The duty ratios of the battery and fuel cell No.1 converters are shown in the first plot in Fig. 18. The output voltage of the battery is constant, so the duty ratio is maintained at a moderate level after compensating for the load fluctuations. The duty ratio induces voltage difference to the inductors, which is the input load to the battery as a load. In the case of higher voltage from the battery, the current is positive and the battery is in discharge mode. As can be concluded from Fig. 18, the step up loads cause the controller to increase the duty ratio with a high rate. These steps to the controller and duty ratio supply the high discharge rate expected from the battery to regulate the bus voltage, because the controller set point of the battery converter is the bus voltage. The fuel cell output voltage varies significantly regarding the applied load, so the controller settles down the duty ratio to various levels. The output duty ratio from the controller is smooth because fuel cell No.1 supplies the low-frequency load demands. The set point of the converter controller for each fuel cell is based on the power demand. The high-level controller defines the required power from each of the fuel cells.

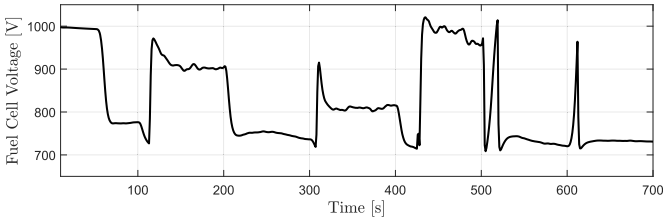

Fig. 17. The fuel cell No.1 voltage responses to the low frequency applied loads.

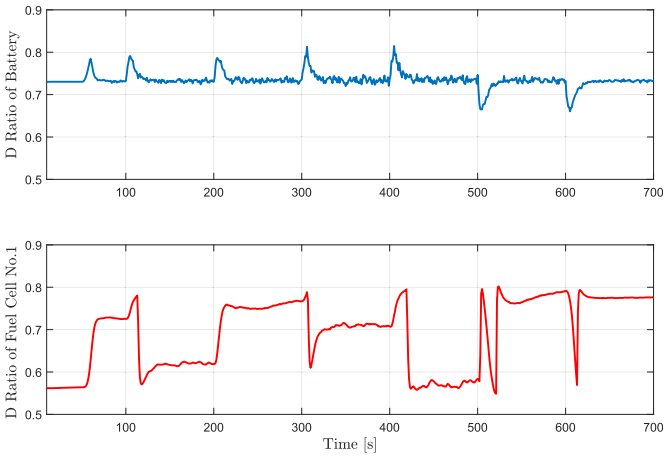

Fig. 18. Duty ratio of the controller to the battery and fuel cell No.1 converter.

The simulation results show the robustness of the power system and controllers in various load levels with oscillations. The system-level modeling approach from auxiliary components of the PEMFC system until the propeller and thruster provide a comprehensive understanding of the system states. For instance, the electromagnetic torque response of the thrusters, the converters duty ratio, battery and fuel cell voltages are monitored. The tuned PEMFC system model with the manufacturer's data for marine application resulted in realistic behavior estimations of the PEMFCs in the model of marine hybrid power systems. The high level control works properly at the start and shut down of the fuel cells, and decomposing the loads to high-frequency and low-frequency. The low level controllers for the converters were robust, and handled the oscillations and step loads properly. There were some dips in the bus voltage for high loads but the deviation is within acceptable tolerance.

The modular modeling approach provides the flexibility of the model in configuration and power capacity size. The fuel cells and battery power range can be changed by the number of cells. Indeed, through the use of proper electrical converters, other power sources such as genset and super capacitors can be integrated into the model's DC bus.

The Vod Adams integration method is used as the solver for this simulation in 20-sim software. The simulation of 700 s is solved in 22 s, which is approximately 31 times faster than real-time in this case. Therefore, the model can be used for real-time applications. The feasibility studies, energy management systems and design optimizations can be performed by the developed model.

4. Conclusion

In this work, a model of the hybrid marine power plant with four PEMFC systems and a battery has been developed by the system-level fidelity. The main aim was to develop a flexible and generic framework that captures the dynamics of the mechanical and electrical components of a hybrid power system with the PEMFC and the battery. The model encompasses auxiliary components of the PEMFC system, power electronics converters, the power management system, converters' low-level control, thrusters and propellers. Indeed, the model has a system-level fidelity, which significantly decreases the computational efforts, while providing a proper estimation of the system's characteristics.

The simulation scenario was designed with step loads and oscillations, demand to the thrusters to test the control robustness and the system performance under various load levels. The power management system with the logic-statements strategy for the start and stop of the fuel cells, with the low pass filter showing a good performance in the starting and the shutting down of the fuel cells while decomposing the load demands to the low and the high frequency. The bus voltage was maintained to the set-point with an acceptable tolerance by the low-level controller of the bidirectional battery converter. This indicates the robustness of the power system. Indeed, the bond graph modular approach and the rule based

PMS provides flexible model in configuration and component power capacity. Indeed, the system-level strategy resulted in real-time in the order of 31, in this specific simulation scenario. It shows the potential of the model to be implemented in repetitive simulation based studies.

In future work, the presented model will be employed in the co-simulation studies for the vessel operations in various cases. The tuned PEMFC system with the real case for marine applications facilitated the feasibility studies for decisions on the size and capabilities of the PEMFC to handle specific load profiles. Indeed, the proposed model can be utilized in design optimization analyses and energy management system studies to find out the proper power capacity range, configuration and control strategy.

Declaration of competing interest

The authors declare that they have no known competing financial interests or personal relationships that could have appeared to influence the work reported in this paper.

Acknowledgement

This work is funded by The Research Council of Norway, SFI Smart Maritime, with project code 237917.

Appendix

The details and parameters of the relations can be found in (Pukrushpan et al., 2004).

$$v_{Nernst} = E^0 - \frac{RT_{st}}{2F} ln\left[\frac{p_{H_2O}}{p_{H_2} \bullet \sqrt{p_{O_2}}}\right]$$

$$E^0 = -\frac{\Delta G}{2F}$$

$$\Delta G = v_{H_2}\mu_{H_2} + v_{O_2}\mu_{O_2} - v_{H_2O}\mu_{H_2O}$$

$$\mu_i = \Delta h_i - T\Delta s_i + RTlog\left(\frac{p_i}{p_{ref}}\right)$$

$$\Delta h_i = h_i^0\left(T - T_{ref}\right)$$

$$\Delta s_i = s_i^0 + M_i c_{pi} log\left(\frac{p_i}{p_{ref}}\right)$$

$$\dot{m}_{out} = \begin{cases} \dfrac{C_D A_T p_{manifold}}{\sqrt{RT_{manifold}}}\left(\dfrac{p_{atm}}{p_{manifold}}\right)^{\frac{1}{\gamma}}\left(\dfrac{2\gamma}{\gamma-1}\left(1-\left(\dfrac{p_{atm}}{p_{manifold}}\right)\right)^{\frac{1}{\gamma}}\right)^{\frac{1}{2}} \\ \text{if } \dfrac{p_{atm}}{p_{manifold}} > \left(\dfrac{2}{\gamma+1}\right)^{\frac{\gamma}{\gamma-1}} \\ \dfrac{C_D A_T p_{manifold}}{\sqrt{RT_{manifold}}}\gamma^{\frac{1}{2}}\left(\dfrac{2}{\gamma+1}\right)^{\frac{\gamma+1}{2(\gamma-1)}} \\ \text{if } \dfrac{p_{atm}}{p_{manifold}} < \left(\dfrac{2}{\gamma+1}\right)\dfrac{\gamma}{\gamma-1} \end{cases}$$

$$C_p = 0.005[\mathrm{j} \cdot kg^{-1} \cdot K^{-1}]$$
$$k_v = 0.0153[V/(rad/s)]$$
$$k_t = 0.0153[N \cdot m/I]$$
$$R_{em} = 0.82[\Omega]$$
$$\eta_{em} = 0.98$$
$$t_m = 0.0125$$

References

Arabul, F.K., Senol, I., Arabul, A.Y., Boynuegri, A.R., 2015. Providing energy management of a fuel cell-battery hybrid electric vehicle. World Academy of Science, Engineering and Technology, International Journal of Electrical, Computer, Energetic, Electronic and Communication Engineering 9 (8), 920–924.

Bagherabadi, K.M., Skjong, S., Pedersen, E., 2022. Dynamic modelling of pem fuel cell system for simulation and sizing of marine power systems. Int. J. Hydrogen Energy 47 (40), 17699–17712. https://doi.org/10.1016/j.ijhydene.2022.03.247.

N. Benyahia, N. Benamrouche, and T. Rekioua, "Modeling, design and simulation of fuel cell modules for small marine applications," in 2012 XXth International Conference on Electrical Machines, pp. 1989–1995, IEEE.

Bø, T.I., Dahl, A.R., Johansen, T.A., Mathiesen, E., Miyazaki, M.R., Pedersen, E., Skjetne, R., Sørensen, A.J., Thorat, L., Yum, K.K., 2015. Marine vessel and power plant system simulator. IEEE Access 3, 2065–2079.

Broenink, J.F., 1999. 20-sim software for hierarchical bond-graph/block-diagram models. Simulat. Pract. Theor. 7 (5–6), 481–492.

W. Chen, K. Tai, M. Lau, A. Abdelhakim, R. R. Chan, A. K. Ådnanes, and T. Tjahjowidodo, "On the modelling of fuel cell-fed power system in electrified vessels," in 2020 IEEE 21st Workshop on Control and Modeling for Power Electronics (COMPEL), pp. 1–8, IEEE.

Geertsma, R., Negenborn, R., Visser, K., Hopman, J., 2017. Design and control of hybrid power and propulsion systems for smart ships: a review of developments. Appl. Energy 194, 30–54.

Ghimire, P., Zadeh, M., Pedersen, E., Thorstensen, J., 2020. Dynamic Modeling, Simulation, and Testing of a Marine Dc Hybrid Power System. IEEE Transactions on Transportation Electrification.

Haxhiu, A., Kyyrä, J., Chan, R., Kanerva, S., 2020. Improved variable dc approach to minimize drivetrain losses in fuel cell marine power systems. IEEE Trans. Ind. Appl. 57 (1), 882–893.

T. Huria, M. Ceraolo, J. Gazzarri, and R. Jackey, "High fidelity electrical model with thermal dependence for characterization and simulation of high power lithium battery cells," in 2012 IEEE International Electric Vehicle Conference, pp. 1–8, IEEE.

Janke, W., 2015. Small-signal transmittances of dc-dc step-down pwm converter in various operation modes. Arch. Electr. Eng. 64 (3), 505–529.

Karnopp, D.C., Margolis, D.L., Rosenberg, R.C., 2012. System Dynamics: Modeling, Simulation, and Control of Mechatronic Systems. John Wiley & Sons.

Lim, C.-o., Park, B.-c., Lee, J.-c., Kim, E.S., Shin, S.-c., 2019. Electric power consumption predictive modeling of an electric propulsion ship considering the marine environment. Int. J. Nav. Archit. Ocean Eng. 11 (2), 765–781.

Nehrir, M.H., Wang, C., 2009. Modeling and Control of Fuel Cells: Distributed Generation Applications, vol. 41. John Wiley & Sons.

Ovrum, E., Dimopoulos, G., 2012. A validated dynamic model of the first marine molten carbonate fuel cell. Appl. Therm. Eng. 35, 15–28.

Pedersen, T.A., Pedersen, E., 2012a. Bond graph modelling of marine power systems.

Math. Comput. Model. Dyn. Syst. 18 (2), 153–173.
Pedersen, T.A., Pedersen, E., 2012b. Bond graph modelling of marine power systems. Math. Comput. Model. Dyn. Syst. 18 (2), 153–173.
Pukrushpan, J.T., Stefanopoulou, A.G., Peng, H., 2004. Control of Fuel Cell Power Systems: Principles, Modeling, Analysis and Feedback Design. Springer Science & Business Media.
J. Schuddebeurs, P. Norman, S. Galloway, G. Burt, J. McDonald, and J. Apsley, "A high fidelity integrated system model for marine power systems," in 2008 2nd Annual IEEE Systems Conference, pp. 1–8, IEEE.
Schuddebeurs, J.D., Norman, P.J., Elders, I.M., Galloway, S.J., Booth, C., Burt, G., Apsley, J., 2010. A solution for improved simulation efficiency of a multi-domain marine power system model. International Journal of Simulation and Process Modelling 6 (1), 67–77.
Z. Shajari, M. Savaghebi, J. M. Guerrero, and M. H. Javidi, "Dynamic performance assessment of ng-mvdc shipboard power system with distributed electric propulsions," in 2020 IEEE Electric Power and Energy Conference (EPEC), pp. 1–7, IEEE.
Skjong, S., Pedersen, E., 2017. A real-time simulator framework for marine power plants with weak power grids. Mechatronics 47, 24–36.
Skjong, S., Rindarøy, M., Kyllingstad, L.T., Æsøy, V., Pedersen, E., 2018. Virtual prototyping of maritime systems and operations: applications of distributed co-simulations. J. Mar. Sci. Technol. 23 (4), 835–853.
Smit, M., 2014. Towards 40 000 hours of operation for nedstack's fcs xxl pem fuel cell stacks. Fuel Cell. Bull. 2014 (8), 12–15.
Sørensen, A.J., 2005. Marine cybernetics. In: Lecture Notes for TMR4240 Marine Control Systems, Dept. Of Marine Tehcnology, NTNU, Trondheim, Norway. http://www.ivt.ntnu.no/imt/courses/tmr4240/.
Van Biert, L., Godjevac, M., Visser, K., Aravind, P., 2016. A review of fuel cell systems for maritime applications. J. Power Sources 327, 345–364.
Vasu, G., Tangirala, A., 2008. Control-orientated thermal model for proton-exchange membrane fuel cell systems. J. Power Sources 183 (1), 98–108.
Vrijdag, A., Stapersma, D., Van Terwisga, T., 2009. Systematic modelling, verification, calibration and validation of a ship propulsion simulation model. J. Marine Eng. Technol. 8 (3), 3–20.
Zahedi, B., 2014. Shipboard Dc Hybrid Power Systems: Modeling, Efficiency Analysis and Stability Control.
Zahedi, B., Norum, E., 2012. Modeling and Simulation of All-Electric Ships with Low-Voltage Dc Hybrid Power Systems, vol. 28, pp. 4525–4537, 10.
Zhang, Z., Guan, C., Liu, Z., 2020. Real-time optimization energy management strategy for fuel cell hybrid ships considering power sources degradation. IEEE Access 8, 87046–87059.
Zhu, W., Shi, J., Abdelwahed, S., 2018. End-to-end system level modeling and simulation for medium-voltage dc electric ship power systems. Int. J. Nav. Archit. Ocean Eng. 10 (1), 37–47.